THE JOURNAL OF PHYSICAL CHEMISTRY LETTERS
A JOURNAL OF THE AMERICAN CHEMICAL SOCIETY

pubs.acs.org/JPCL

Letter

Superlattice Surface Lattice Resonances in Plasmonic Nanoparticle Arrays with Patterned Dielectrics

Danqing Wang, Jingtian Hu, George C. Schatz, and Teri W. Odom*

Cite This: *J. Phys. Chem. Lett.* 2023, 14, 8525−8530

Read Online

ACCESS | Metrics & More | Article Recommendations | Supporting Information

ABSTRACT: This paper describes how two-dimensional plasmonic nanoparticle lattices covered with microscale arrays of dielectric patches can show superlattice surface lattice resonances (SLRs). These optical resonances originate from multiscale diffractive coupling that can be controlled by the periodicity and size of the patterned dielectrics. The features in the optical dispersion diagram are similar to those of index-matched microscale arrays of metal nanoparticle lattices, having the same lateral dimensions as the dielectric patches. With an increase in nanoparticle size, superlattice SLRs can also support quadrupole excitations with distinct dispersion diagrams. The tunable optical band structure enabled by patterned dielectrics on plasmonic nanoparticle arrays offers prospects for enhanced nonlinear optics, nanoscale lasing, and engineered parity-time symmetries.

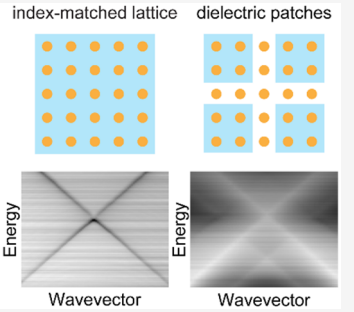

Electronic band structures of solids describe the range of allowed energy levels of electrons as a function of momentum.[1] Similarly, optical band structures depict electromagnetic modes of photonic systems. Compared to bulk materials whose optical responses are determined by intrinsic properties of the materials, photonic materials exhibit properties that depend on geometric structure, and their associated optical dispersion diagrams can be engineered for applications in small-scale optical cavities, topological photonics, and non-Hermitian photonics.[2−6] The integration of multiple length scales with a nanosystem offers an approach for manipulating optical interactions and enabling applications in moiré photonic flat bands, enhanced nonlinear optics, and large-scale photonic circuits.[7−10] The nanofabrication processes required, however, multistep top-down lithography or bottom-up self-assembly.[11−14]

Two-dimensional (2D) periodic arrays of plasmonic nanoparticles (NPs) provide a platform for modulating the optical coupling between individual units.[15−18] Surface lattice resonances (SLRs, also termed lattice plasmons) result from the interactions between the localized surface plasmons (LSPs) of individual NPs and diffractive modes defined by the lattice spacing (a_0) and symmetry.[19−21] Tuning the size and shape of NPs results in either dipolar or quadrupolar LSPs with distinct charge distributions, and varying the lattice geometry and symmetry mediates coupling from the LSP to different diffractive mode orders.[22−26] In addition to NP lattices with a single periodicity a_0, microscale patches of NPs that sustain two periodicities, finite-sized lattices grouped into larger arrays with patch spacing (A_0), can generate superlattice SLRs, where A_0 is an order of magnitude larger than the submicrometer interparticle spacing.[27−30] These multiple resonances arise from the coupling between SLR modes of a single NP patch and the high-order Bragg modes from the microscale patch spacing; applications have included multimodal nanolasing and biomedical imaging.[31−34]

The open-cavity architecture of plasmonic NP lattices enables tunability of the surrounding dielectric environment. In NP lattices, the highest-quality SLRs with ultranarrow line widths (full width at half-maximum of <5 nm) are formed when the superstrate and the substrate around the NP lattices are index-matched.[35,36] Tailoring the local dielectric environment by patterning polymer blocks around individual NPs in a lattice has been used to manipulate the wavefront at the SLR resonance for optical focusing and imaging.[37−39] Whether larger dielectric patches on 2D NP lattices could produce equivalent superlattice SLR properties like that from plasmonic NP patch arrays in a uniform dielectric environment is unknown but would address drawbacks in their multistep fabrication process that involves lithography, etching, and metal deposition.[13,40]

Here we show that superlattice SLRs can be generated from plasmonic NP lattices covered with rationally designed microscale arrays of dielectric patches. First, by varying the 2D dielectric patch periodicity, we systematically tuned SLR wavelengths at the Γ point and their associated optical dispersion diagrams. Next, by reducing the microscale array symmetry of the patterned dielectrics from 2D to one-dimensional (1D), we realized switchable resonances between

Received: August 2, 2023
Accepted: September 13, 2023
Published: September 18, 2023

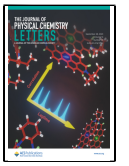

https://doi.org/10.1021/acs.jpclett.3c02158
J. Phys. Chem. Lett. 2023, 14, 8525−8530

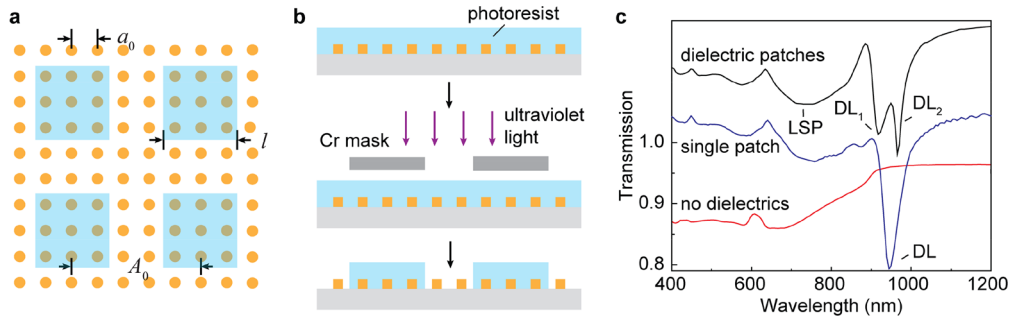

Figure 1. 2D Au nanoparticle lattices patterned with microscale dielectric patches to achieve superlattice SLRs. (a) Scheme of a Au NP lattice patterned with 2D photoresist patches with interparticle spacing a_0, patch side length l, and patch periodicity A_0. (b) Scheme of fabrication of 2D photoresist patches on Au NP arrays on fused silica by contact photolithography. (c) Simulated transmission spectra at normal incidence without dielectrics (red curve), with a micrometer-sized photoresist patch (blue curve; l = 6 μm), and with a 2D array of photoresist patches covering the Au NPs (black curve). Patch periodicity was (l, A_0) = (6 μm, 9 μm), and NP periodicity was a_0 = 600 nm with NP diameter d = 160 nm and height h = 60 nm. The LSP wavelength of the Au NPs is λ_{LSP} = 736 nm. Transmission curves were offset by 0.1 from top to bottom.

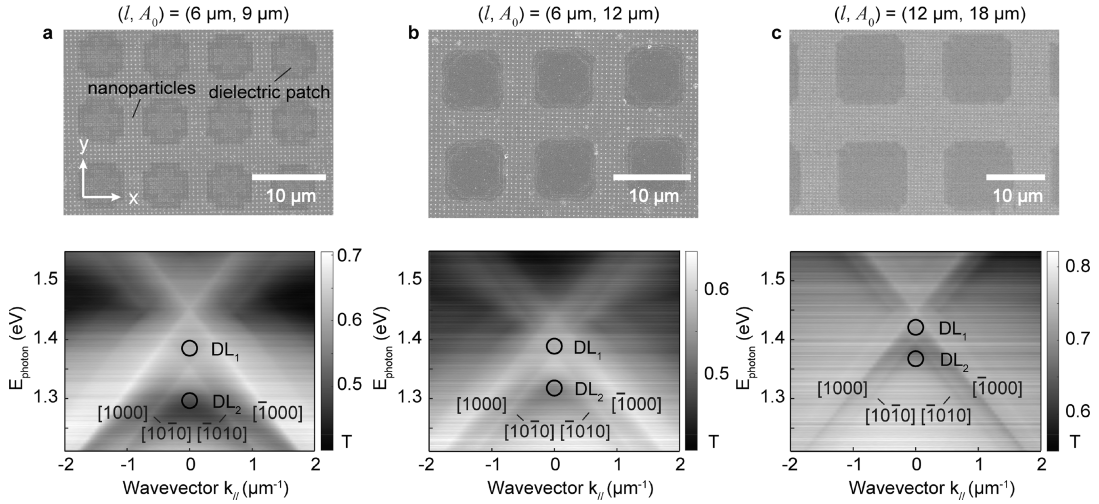

Figure 2. Tunable optical band structures of 2D Au NP lattices covered with photoresist patches having different periodicities. Scanning electron microscopy (SEM) images and measured dispersion diagrams of NP lattices with patterned dielectrics under TE polarization with (a) patch periodicity (l, A_0) = (6 μm, 9 μm), (b) patch periodicity (l, A_0) = (6 μm, 12 μm), and (c) patch periodicity (l, A_0) = (12 μm, 18 μm). The thickness of the dielectric patches was ~200 nm. In the SEM images, the regions between patches appeared brighter than those of the dielectric-coated patches, which can be attributed to increased electron scattering by metal NPs.

single-lattice and superlattice SLRs by controlling the light polarization. Finally, by increasing the NP size, we found that superlattice SLRs with quadrupolar character could be supported with a mode dispersion behavior distinct from that of dipolar superlattice SLRs. Patterned dielectric patches enable a simple degree of freedom to tune multiscale optical responses in 2D nanophotonics.

Figure 1 shows how patterned dielectric patches on plasmonic NP lattices can produce superlattice SLRs. Contact photolithography with a photomask having micrometer-sized Cr patches (side length l and periodicity A_0) was used to generate photoresist patches on Au NP lattices on a fused silica substrate (refractive index n = 1.48) (Figure 1a). The plasmonic lattices were first fabricated using our large-scale nanofabrication procedures of PEEL and SANE,[13] where first a thin photoresist film (n = 1.5) was spin-cast on top of the NP lattices (Figure 1b and Figure S1). Ultraviolet light exposure with the Cr photomask followed by photoresist development created photoresist patches on NP lattices (Methods). Measured height profiles (Figure S2) indicate that the exposed Au NPs between the dielectric patches had no residual photoresist.

Finite-difference time-domain (FDTD) methods were used to model and compare the optical resonances of plasmonic NP lattices with and without dielectric patches. Different from a single index-matched, micrometer-sized patch (l = 6 μm) on Au NPs that supports a dipolar SLR at the Γ point [λ_{DL} = 944 nm (Figure 1c, blue curve)], Au NPs not covered with a dielectric (air only) have a high index contrast between the superstrate and the fused silica substrate and cannot sustain SLRs (red curve). In NP lattices patterned with photoresist patches (periodicity A_0 = 9 μm), the N = 15 and N = 14 orders of Bragg modes from A_0 induced superlattice SLR modes at λ_{DL1} = 923 nm and λ_{DL2} = 965 nm (black curve). The simulated transmission spectra show resonance features similar to those in index-matched arrays of NP lattices (Figure S3). Charge distribution plots indicate dipolar oscillations of Au NPs at DL_1 and DL_2 (Figure S4a,b). At DL_1, all NPs oscillate with the same phase, similar to the case in a single-periodicity lattice. The near-field distribution at DL_2 is modified by the microscale patch−patch coupling and exhibits an overall phase shift of π across one dielectric patch (Figure S4c,d). Despite the index-mismatched regions between dielectric patches that cannot support SLRs, strong optical fields are maintained in

https://doi.org/10.1021/acs.jpclett.3c02158
J. Phys. Chem. Lett. 2023, 14, 8525−8530

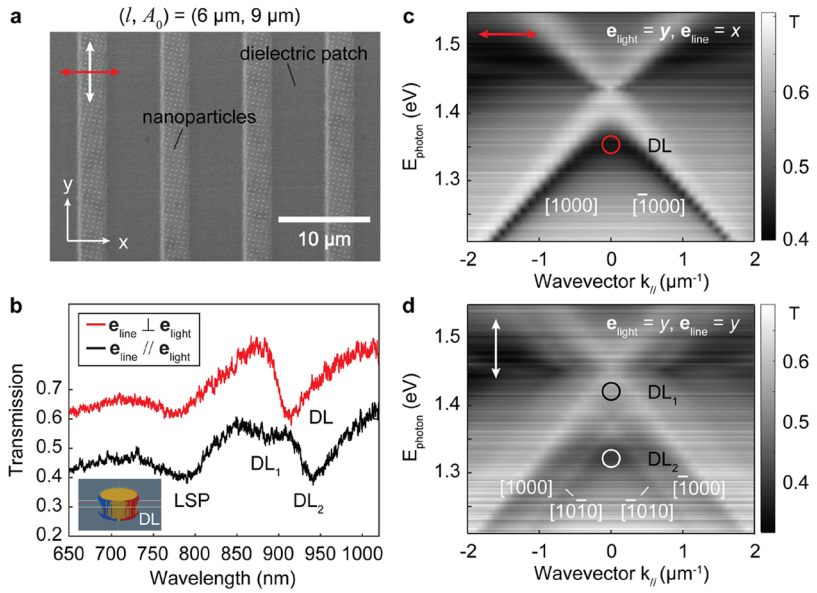

Figure 3. Polarization-dependent properties of 2D Au NP lattices with patterned dielectric lines. (a) SEM image of Au NP arrays (d = 160 nm, h = 60 nm) patterned with photoresist line patches. The patch periodicity was (l, A_0) = (6 μm, 9 μm). Note that the line axis was not commensurate with the underlying NP lattice and the angular offset was ~12°. (b) Polarization-dependent transmission spectra, where the red and black curves correspond to light polarization $\mathbf{e}_{light}$ perpendicular and parallel to line axis $\mathbf{e}_{line}$, respectively. The charge distribution plot shows dipolar oscillations in the Au NPs, where positive and negative charges are colored red and blue, respectively. (c and d) Measured optical band structures under TE polarization. The arrows indicate the direction of $\mathbf{e}_{line}$ with respect to $\mathbf{e}_{light}$.

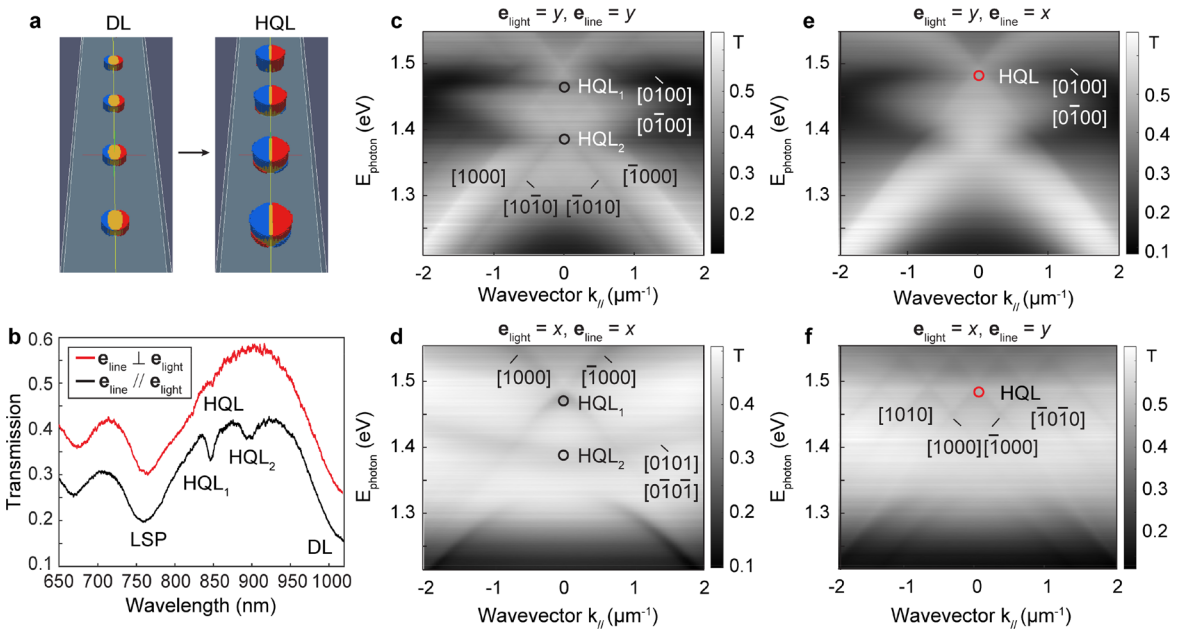

Figure 4. Quadrupolar superlattice SLRs in patterned arrays of large Au NPs. (a) Plots of charge distributions of Au NPs patterned with photoresist line patches at DL and HQL resonances for comparison. For Au NPs, d = 160 nm and h = 60 nm for DL modes (left) and d = 260 nm and h = 120 nm for HQL modes (right); a_0 = 600 nm. (b) Measured transmission spectra at normal incidence, where red and black curves represent the excitation polarization $\mathbf{e}_{light}$ being perpendicular and parallel to line axis $\mathbf{e}_{line}$, respectively. Measured optical band structures when $\mathbf{e}_{light}$ was (c and d) parallel and (e and f) perpendicular to $\mathbf{e}_{line}$.

NP lattices with patterned dielectrics, and the $|E|$ intensity close to the vicinity of NPs is comparable to that of a singly spaced lattice (Figure S4e).

Figure 2 shows the measured optical band structures of plasmonic NP lattices supporting dipolar SLRs patterned with dielectric patches in different spacings. Under transverse electric (TE) polarization (along y), DL_1 and DL_2 appeared at the band edge at zero wavevector ($k_{||}$ = 0) for a patch periodicity A_0 = 9 μm (Figure 2a). In reciprocal space, these superlattice SLRs correspond to different Bragg orders that combine the wavevectors defined by various lattice spacings. Here, the Bragg modes can be indexed as $[k_x\ k_y\ k_x'\ k_y']$, where k_x (k_y) and k_x' (k_y') represent grating vectors from the NP spacing ($k = 2\pi/a_0$) and patch spacing ($k' = 2\pi/A_0$), respectively. DL_1 is a result of the N = 15 order Bragg modes from patch spacing A_0 = 9 μm, which is equivalent to

https://doi.org/10.1021/acs.jpclett.3c02158
J. Phys. Chem. Lett. 2023, 14, 8525−8530

the fundamental Bragg mode from NP spacing a_0 = 600 nm. Hence, under TE polarization, the dispersion of superlattice mode DL_1 followed the fundamental modes [1000] and [$\bar{1}$000]. DL_2 originated from the N = 14 order Bragg mode from A_0, and the mode dispersion of DL_2 followed the satellite modes [10$\bar{1}$0] and [$\bar{1}$010].

Microscale photoresist patterns were tailored by using different Cr masks in contact photolithography. Increasing the periodicity of photoresist patches from A_0 = 9 to 12 μm resulted in more high-order Bragg modes with smaller energy separations ($E = hc/\lambda$, where h is Planck's constant and c is the speed of light) and hence a blue-shifted DL_2 (Figure 2b). We further increased the patch spacing to A_0 = 18 μm while keeping the ratio of l to A_0 constant. The SLR of a single lattice coupled to even higher-order Bragg modes from A_0 (N = 30 and N = 29) and produced a smaller energy separation between DL_1 and DL_2 (Figure 2c). In the transmission spectra, the decreased transmission intensity at shorter wavelengths can be attributed to optical Rayleigh scattering[41] by the microscale dielectric blocks (Figures S5 and S6). With a decrease in A_0, the wavelength separation between DL_1 and DL_2 became larger, and only weak mode DL_2 was observed in the simulation for $A_0 = 10a_0$ [A_0 = 6 μm (Figure S7)]. Notably, photoresist patches can be easily rinsed off with organic solvents, which allows for reconfigurable control[38] of the optical responses.

Unlike 2D dielectric patches on NP lattices with 4-fold rotational symmetry, NP lattices covered with dielectric patches having reduced symmetry enable access to polarization-dependent optical properties. Figure 3a shows photoresist line patches on the 2D Au NP lattices. When Au NPs exhibit dipolar charge oscillations along a light polarization direction $\mathbf{e}_{light}$, the NPs aligned perpendicular to this direction can couple with each other.[27] Similarly, when the line-axis direction $\mathbf{e}_{line}$ is parallel to $\mathbf{e}_{light}$ (along y), microscale periodicity A_0 along the NP coupling direction leads to polarization- and orientation-dependent optical responses (Figure 3b). In experiments, despite an angular offset of 12° between the line axis of dielectric patches and the high-symmetry axis of NP lattices, we observed a single resonance DL when $\mathbf{e}_{light}$ was perpendicular to $\mathbf{e}_{line}$, and the dispersion followed the [1000] and [$\bar{1}$000] Bragg modes under TE polarization (Figure 3c). In contrast, rotating the line axis 90° under TE polarization produced multiple superlattice SLR resonances, DL_1 and DL_2. In the dispersion diagram, DL_1 followed the fundamental Bragg modes [1000] and [$\bar{1}$000], and DL_2 followed the satellite modes [10$\bar{1}$0] and [$\bar{1}$010] (Figure 3d), consistent with the dispersion behavior of superlattice DLs in an index-matched environment.[33]

In addition to SLRs based on dipolar resonances, hybrid quadrupole lattice plasmons (HQLs) are accessible in plasmonic lattices with increased NP size, where NPs exhibit overall quadrupolar charge oscillations with a non-zero net dipole moment[22,24] as a result of phase retardation effects (Figure 4a). We patterned 2D photoresist patches on arrays of large Au NPs (d = 260 nm, h = 120 nm) and observed multiple superlattice HQL modes (Figure S8). Distinct dispersion diagrams were observed for NP lattices with patterned dielectric line patches. When $\mathbf{e}_{light}$ was parallel to $\mathbf{e}_{line}$, both HQL_1 and HQL_2 appeared in the transmission spectrum (Figure 4b and Figure S9). The dispersion of HQL_1 followed the Bragg modes [0100] and [0$\bar{1}$00] under TE polarization ($\mathbf{e}_{light} = y$) and [1000] and [$\bar{1}$000] under transverse magnetic (TM) polarization [$\mathbf{e}_{light} = x$ (Figure 4c,d)], similar to HQLs in a single-periodicity lattice.[24] In contrast to HQL_1, the dispersion of mode HQL_2 followed [10$\bar{1}$0] and [$\bar{1}$010] modes under TE polarization and [0101] and [0$\bar{1}$0$\bar{1}$] modes under TM polarization. Changing the light polarization to be perpendicular to the dielectric lines produced only a single HQL resonance with a dispersive behavior similar to that of HQL_1 (Figure 4e,f). Interestingly, Figure 4f shows that new superlattice HQLs appeared at higher energies compared to the fundamental Bragg modes [1000] and [$\bar{1}$000] (e.g., [1010] and [$\bar{1}$0$\bar{1}$0] modes), while the superlattice DLs dominated at lower energies (e.g., [10$\bar{1}$0] and [$\bar{1}$010] modes),[33] which could be attributed to higher-energy quadrupolar LSPs[24] in Au NPs compared to dipolar LSPs.

In summary, we demonstrated that patterning microscale dielectric patches on plasmonic NP lattices enables the formation of superlattice SLRs that are similar to those from patterned microscale NP lattices in a uniform refractive index environment. This work opens prospects for manipulation of optical band structures of metal NP lattices via patterned dielectric superstrates, which can benefit solid-state optical devices and integrated photonic circuits. Also, microscale patterning with dielectrics provides a general approach for modulating other 2D nanophotonic systems for metalens imaging, chirality engineering, and long-range optical coupling. We anticipate that incorporating gain media such as dye molecules into the dielectric blocks can induce side-by-side control of gain and loss regions in plasmonic lattices for engineered parity-time symmetry. Materials systems with rationally tailored multiscale optical interactions offer the potential for enhanced nonlinear optics, nanoscale lasing, and nontrivial topological states.

METHODS

Fabrication of Au NP Lattices with Dielectric Patches. Lattices of Au NPs were fabricated with a large-scale nanofabrication process known as PEEL.[13] Briefly, we generated periodic arrays of photoresist posts on a Si wafer by phase-shifting photolithography using a poly(dimethylsiloxane) (PDMS) mask with pattern periodicity a_0 = 600 nm. Free-standing Au nanohole films were prepared after Cr deposition and lift-off of photoresist posts, etching through Si to create cylindrical pits, Au deposition, and lift-off of the Au film by etching the sacrificial Cr layer. Metal deposition through the nanohole films followed by removal of the Au film with scotch tape produced NP lattices on fused silica substrates. To fabricate the microscale dielectric patches, we spin-cast a photoresist thin film (MICROPOSIT S1805 positive photoresist) on the Au NP arrays at a spin speed of 3000 rpm (film thickness of ~200 nm) and performed contact photolithography with a Cr mask whose patterns determined the dielectric patch size.

Optical Band Structure Measurements. We characterized optical band structures of plasmonic NP lattices by compiling transmission spectra at different incident angles θ_I. In the experiments, samples were placed at the center of a program-controlled rotational stage. The transmission spectra were collected by sweeping various incident angles θ_I from −20° to 20° in 1° increments using an automated, home-built National Instruments Lab-VIEW program. Optical band structures of the patterned NP lattices in wavelength (λ)−incidence angle (θ_I) units can be transferred into energy (E)−wavevector ($k_{||}$) format by the equations $E = hc/\lambda$ and $k_{||} = (2\pi/\lambda) \sin \theta_I$, where c is the speed of light.

https://doi.org/10.1021/acs.jpclett.3c02158
J. Phys. Chem. Lett. 2023, 14, 8525−8530

Finite-Difference Time-Domain (FDTD) Simulations. FDTD calculations with commercial software (FDTD solution, Lumerical Inc., Vancouver, BC) were used to model the linear optical properties of patterned Au NP lattices. The optical constants of Au were taken from Johnson and Christy measurements (400−1020 nm).[42] We used a uniform mesh size of 4 nm (x, y, and z) for the accuracy of electromagnetic field calculations within the metal regions. The charge distribution plots were extracted from the E_x, E_y, and E_z values at different grid sites in the simulations and processed in Paraview software.

■ ASSOCIATED CONTENT

Supporting Information

The Supporting Information is available free of charge at https://pubs.acs.org/doi/10.1021/acs.jpclett.3c02158.

> Surface lattice resonance in photoresist-coated Au nanoparticle arrays, atomic force microscopy image of patterned nanoparticle lattices, comparison of simulated superlattice SLRs, near-field and charge distributions of superlattice SLRs in patterned Au nanoparticles, measured transmission spectra of dipolar superlattice SLRs, transmission spectra of a patterned PDMS slab on nanoparticle lattices and on a silica substrate, hybrid quadrupole lattice plasmons in nanoparticle lattices with patterned dielectrics, and polarization- and orientation-dependent hybrid quadrupole lattice plasmons (PDF)

■ AUTHOR INFORMATION

Corresponding Author

Teri W. Odom − *Department of Chemistry, Graduate Program in Applied Physics, and Department of Materials Science and Engineering, Northwestern University, Evanston, Illinois 60208, United States;* orcid.org/0000-0002-8490-292X; Email: todom@northwestern.edu

Authors

Danqing Wang − *Graduate Program in Applied Physics, Northwestern University, Evanston, Illinois 60208, United States;* orcid.org/0000-0002-7369-1944

Jingtian Hu − *Department of Chemistry, Northwestern University, Evanston, Illinois 60208, United States;* orcid.org/0000-0002-0528-6250

George C. Schatz − *Department of Chemistry and Graduate Program in Applied Physics, Northwestern University, Evanston, Illinois 60208, United States;* orcid.org/0000-0001-5837-4740

Complete contact information is available at: https://pubs.acs.org/10.1021/acs.jpclett.3c02158

Author Contributions

D.W., J.H., and T.W.O. conceived the idea of patterned nanoparticle lattice studies. D.W. fabricated the devices, carried out the optical measurements, and performed numerical simulations of the optical band structures and near-field distributions. J.H. contributed to the photoresist embossing and contact lithography patterning process. T.W.O. and G.C.S. guided experimental and theoretical investigations. D.W., G.C.S., and T.W.O. analyzed the data and wrote the manuscript. All authors commented on and revised the manuscript.

Notes

The authors declare no competing financial interest.

■ ACKNOWLEDGMENTS

This work was supported by the National Science Foundation (NSF) under Grants DMR-1904385 and DMR-2207215 (D.W., G.C.S., and T.W.O.) and the Vannevar Bush Faculty Fellowship from the Department of Defense (DOD N00014-17-1-3023) (T.W.O.). This work made use of the NUFAB facility of Northwestern University's NUANCE Center, which has received support from the SHyNE Resource (NSF ECCS-2025633), the International Institute for Nanotechnology (IIN), and Northwestern's MRSEC program (NSF DMR-1720139). This research was supported in part by the Quest high-performance computing facility at Northwestern University, which is jointly supported by the Office of the Provost, the Office for Research, and Northwestern University Information Technology. The authors thank Dr. Jun Guan for helpful discussions.

■ REFERENCES

(1) Ashcroft, N. W.; Mermin, N. D. *Solid State Physics*; Saunders College: Philadelphia, 1976; Appendix N 2010, Vol. *166*.

(2) Joannopoulos, J. D.; Johnson, S. G.; Winn, J. N.; Meade, R. D. *Photonic Crystals: Molding the Flow of Light*, 2nd ed.; 2008; pp 1−286.

(3) Feng, L.; El-Ganainy, R.; Ge, L. Non-Hermitian photonics based on parity−time symmetry. *Nat. Photonics* **2017**, *11* (12), 752−762.

(4) Zhao, H.; Qiao, X.; Wu, T.; Midya, B.; Longhi, S.; Feng, L. Non-Hermitian topological light steering. *Science* **2019**, *365* (6458), 1163−1166.

(5) Price, H.; Chong, Y.; Khanikaev, A.; Schomerus, H.; Maczewsky, L. J.; Kremer, M.; Heinrich, M.; Szameit, A.; Zilberberg, O.; Yang, Y.; et al. Roadmap on topological photonics. *JPhys Photonics* **2022**, *4* (3), No. 032501.

(6) Peng, B.; Özdemir, Ş. K.; Lei, F.; Monifi, F.; Gianfreda, M.; Long, G. L.; Fan, S.; Nori, F.; Bender, C. M.; Yang, L. Parity−time-symmetric whispering-gallery microcavities. *Nat. Phys.* **2014**, *10* (5), 394−398.

(7) Zhu, S.-n.; Zhu, Y.-y.; Ming, N.-b. Quasi-phase-matched third-harmonic generation in a quasi-periodic optical superlattice. *Science* **1997**, *278* (5339), 843−846.

(8) Elshaari, A. W.; Pernice, W.; Srinivasan, K.; Benson, O.; Zwiller, V. Hybrid integrated quantum photonic circuits. *Nat. Photonics* **2020**, *14* (5), 285.

(9) Sunku, S. S.; Ni, G. X.; Jiang, B. Y.; Yoo, H.; Sternbach, A.; McLeod, A. S.; Stauber, T.; Xiong, L.; Taniguchi, T.; Watanabe, K.; Kim, P.; Fogler, M. M.; Basov, D. N. Photonic crystals for nano-light in moire graphene superlattices. *Science* **2018**, *362* (6419), 1153−1156.

(10) Dong, K.; Zhang, T.; Li, J.; Wang, Q.; Yang, F.; Rho, Y.; Wang, D.; Grigoropoulos, C. P.; Wu, J.; Yao, J. Flat bands in magic-angle bilayer photonic crystals at small twists. *Physical review letters* **2021**, *126* (22), No. 223601.

(11) Macfarlane, R. J.; Lee, B.; Jones, M. R.; Harris, N.; Schatz, G. C.; Mirkin, C. A. Nanoparticle superlattice engineering with DNA. *Science* **2011**, *334* (6053), 204−8.

(12) Ross, M. B.; Ku, J. C.; Vaccarezza, V. M.; Schatz, G. C.; Mirkin, C. A. Nanoscale form dictates mesoscale function in plasmonic DNA-nanoparticle superlattices. *Nat. Nanotechnol* **2015**, *10* (5), 453−8.

(13) Henzie, J.; Lee, M. H.; Odom, T. W. Multiscale patterning of plasmonic metamaterials. *Nat. Nanotechnol.* **2007**, *2* (9), 549−54.

(14) Murai, S.; Abujetas, D. R.; Liu, L.; Castellanos, G. W.; Giannini, V.; Sánchez-Gil, J. A.; Tanaka, K.; Gómez Rivas, J. Engineering bound states in the continuum at telecom wavelengths with non-bravais lattices. *Laser Photonics Rev.* **2022**, *16* (11), No. 2100661.

(15) Wang, D.; Guan, J.; Hu, J.; Bourgeois, M. R.; Odom, T. W. Manipulating Light-Matter Interactions in Plasmonic Nanoparticle Lattices. *Acc. Chem. Res.* **2019**, *52* (11), 2997−3007.
(16) Kravets, V. G.; Kabashin, A. V.; Barnes, W. L.; Grigorenko, A. N. Plasmonic Surface Lattice Resonances: A Review of Properties and Applications. *Chem. Rev.* **2018**, *118* (12), 5912−5951.
(17) Cherqui, C.; Bourgeois, M. R.; Wang, D.; Schatz, G. C. Plasmonic Surface Lattice Resonances: Theory and Computation. *Acc. Chem. Res.* **2019**, *52* (9), 2548−2558.
(18) Wang, W.; Ramezani, M.; Väkeväinen, A. I.; Törmä, P.; Rivas, J. G.; Odom, T. W. The rich photonic world of plasmonic nanoparticle arrays. *Mater. Today* **2018**, *21* (3), 303−314.
(19) Evlyukhin, A. B.; Reinhardt, C.; Zywietz, U.; Chichkov, B. N. Collective resonances in metal nanoparticle arrays with dipole-quadrupole interactions. *Phys. Rev. B* **2012**, *85*, No. 245411.
(20) Auguie, B.; Bendana, X. M.; Barnes, W. L.; Garcia de Abajo, F. J. Diffractive arrays of gold nanoparticles near an interface: Critical role of the substrate. *Phys. Rev. B* **2010**, *82* (15), No. 155447.
(21) Kravets, V. G.; Schedin, F.; Grigorenko, A. N. Extremely narrow plasmon resonances based on diffraction coupling of localized plasmons in arrays of metallic nanoparticles. *Phys. Rev. Lett.* **2008**, *101* (8), No. 087403.
(22) Yang, A.; Hryn, A. J.; Bourgeois, M. R.; Lee, W. K.; Hu, J.; Schatz, G. C.; Odom, T. W. Programmable and reversible plasmon mode engineering. *Proc. Natl. Acad. Sci. U. S. A.* **2016**, *113* (50), 14201−14206.
(23) Sakai, K.; Nomura, K.; Yamamoto, T.; Omura, T.; Sasaki, K. Quadrupole lattice resonances in plasmonic crystal excited by cylindrical vector beams. *Sci. Rep.* **2016**, *6*, No. 34967.
(24) Wang, D.; Bourgeois, M. R.; Lee, W. K.; Li, R.; Trivedi, D.; Knudson, M. P.; Wang, W.; Schatz, G. C.; Odom, T. W. Stretchable Nanolasing from Hybrid Quadrupole Plasmons. *Nano Lett.* **2018**, *18* (7), 4549−4555.
(25) Zhou, W.; Dridi, M.; Suh, J. Y.; Kim, C. H.; Co, D. T.; Wasielewski, M. R.; Schatz, G. C.; Odom, T. W. Lasing action in strongly coupled plasmonic nanocavity arrays. *Nat. Nanotechnol.* **2013**, *8* (7), 506−11.
(26) Freire-Fernández, F.; Cuerda, J.; Daskalakis, K. S.; Perumbilavil, S.; Martikainen, J.-P.; Arjas, K.; Törmä, P.; van Dijken, S. Magnetic on−off switching of a plasmonic laser. *Nat. Photonics* **2022**, *16* (1), 27−32.
(27) Wang, D.; Yang, A. K.; Hryn, A. J.; Schatz, G. C.; Odom, T. W. Superlattice Plasmons in Hierarchical Au Nanoparticle Arrays. *Acs Photonics* **2015**, *2* (12), 1789−1794.
(28) Guo, R.; Hakala, T. K.; Torma, P. Geometry dependence of surface lattice resonances in plasmonic nanoparticle arrays. *Phys. Rev. B* **2017**, *95* (15), 155423.
(29) Cuartero-Gonzalez, A.; Sanders, S.; Zundel, L.; Fernandez-Dominguez, A. I.; Manjavacas, A. Super- and Subradiant Lattice Resonances in Bipartite Nanoparticle Arrays. *ACS Nano* **2020**, *14* (9), 11876−11887.
(30) Schokker, A. H.; Koenderink, A. F. Lasing in quasi-periodic and aperiodic plasmon lattices. *Optica* **2016**, *3* (7), 686−693.
(31) Hill, M. T.; Gather, M. C. Advances in small lasers. *Nat. Photonics* **2014**, *8* (12), 908−918.
(32) Ma, R. M.; Oulton, R. F. Applications of nanolasers. *Nat. Nanotechnol.* **2019**, *14* (1), 12−22.
(33) Wang, D.; Yang, A.; Wang, W.; Hua, Y.; Schaller, R. D.; Schatz, G. C.; Odom, T. W. Band-edge engineering for controlled multi-modal nanolasing in plasmonic superlattices. *Nat. Nanotechnol.* **2017**, *12* (9), 889−894.
(34) Guan, J.; Park, J.-E.; Deng, S.; Tan, M. J.; Hu, J.; Odom, T. W. Light−Matter Interactions in Hybrid Material Metasurfaces. *Chem. Rev.* **2022**, *122* (19), 15177−15203.
(35) Deng, S.; Li, R.; Park, J. E.; Guan, J.; Choo, P.; Hu, J.; Smeets, P. J. M.; Odom, T. W. Ultranarrow plasmon resonances from annealed nanoparticle lattices. *Proc. Natl. Acad. Sci. U. S. A.* **2020**, *117* (38), 23380−23384.
(36) Yang, A.; Hoang, T. B.; Dridi, M.; Deeb, C.; Mikkelsen, M. H.; Schatz, G. C.; Odom, T. W. Real-time tunable lasing from plasmonic nanocavity arrays. *Nat. Commun.* **2015**, *6*, 6939.
(37) Ao, X.; Wang, D.; Odom, T. W. Enhanced Fields in Mirror-Backed Low-Index Dielectric Structures. *ACS Photonics* **2019**, *6* (11), 2612−2617.
(38) Hu, J.; Wang, D.; Bhowmik, D.; Liu, T.; Deng, S.; Knudson, M. P.; Ao, X.; Odom, T. W. Lattice-Resonance Metalenses for Fully Reconfigurable Imaging. *ACS Nano* **2019**, *13* (4), 4613−4620.
(39) Lee, M. H.; Huntington, M. D.; Zhou, W.; Yang, J. C.; Odom, T. W. Programmable soft lithography: solvent-assisted nanoscale embossing. *Nano Lett.* **2011**, *11* (2), 311−5.
(40) Zundel, L.; May, A.; Manjavacas, A. Lattice resonances induced by periodic vacancies in arrays of nanoparticles. *ACS Photonics* **2021**, *8* (1), 360−368.
(41) Seinfeld, J. H.; Pandis, S. N. *Atmospheric chemistry and physics: from air pollution to climate change*; John Wiley & Sons, 2016.
(42) Johnson, P. B.; Christy, R. W. Optical Constants of Noble Metals. *Phys. Rev. B* **1972**, *6* (12), 4370−4379.

https://doi.org/10.1021/acs.jpclett.3c02158
J. Phys. Chem. Lett. 2023, 14, 8525−8530